

Dipole oscillations of a Fermi gas in a disordered trap: damping and localization

L. PEZZÈ, B. HAMBRECHT and L. SANCHEZ-PALENCIA^(a)

Laboratoire Charles Fabry de l'Institut d'Optique, CNRS and Univ. Paris-Sud, Campus Polytechnique, RD 128, F-91127 Palaiseau cedex, France

PACS 03.75.-b – Matter waves
 PACS 03.75.Ss – Degenerate Fermi gases

Abstract. - We theoretically study the dipole oscillations of an ideal Fermi gas in a disordered trap. We show that even weak disorder induces strong damping of the oscillations and we identify a metal-insulator crossover. For very weak disorder, we show that damping results from a dephasing effect related to weak random perturbations of the energy spectrum. For increasing disorder, we show that the Fermi gas crosses over to an insulating regime characterized by strong-damping due to the proliferation of localized states.

Introduction. – Ultracold atoms in disordered potentials are currently attracting considerable interest. They offer unprecedented possibilities to revisit many open questions on disordered quantum systems with accurate experimental control of relevant parameters and original measurement techniques. The spectacular progress achieved in disordered Bose-Einstein condensates (BECs) have recently lead to the first direct observation of Anderson localization of matter-waves [1,2], showing remarkable agreement with theoretical calculations [3,4]. A future challenge to ultracold gases is the production of disordered Fermi systems. Even better than Bose gases, they would mimic systems of direct relevance for condensed-matter physics, such as dirty superconductors [5] and granular metals [6]. Moreover, ultracold gases provide original insights on transport phenomena without direct counterparts in traditional condensed-matter physics. For instance, ultracold atoms trapped in harmonic potentials may undergo dipole oscillations – i.e. oscillations of the center of mass (CM) – that can be observed for tens of periods. Since dipole oscillations are undamped in pure harmonic traps, irrespective to the nature of particles, temperature and interactions [7], damping results from the influence of external potentials only. Hence, dipole oscillations have been used to characterize several properties of quantum gases [8,9]. These include bosonic quantum degeneracy [10], inhibition of transport of Bose gases in one-dimensional (1D) optical lattices [11], fermionic band

insulators in periodic lattices [12,13], localization of spin-polarized fermions in disorder-free aperiodic lattices [14], and interaction-controlled transport of fermions in optical lattices [15], just to mention a few.

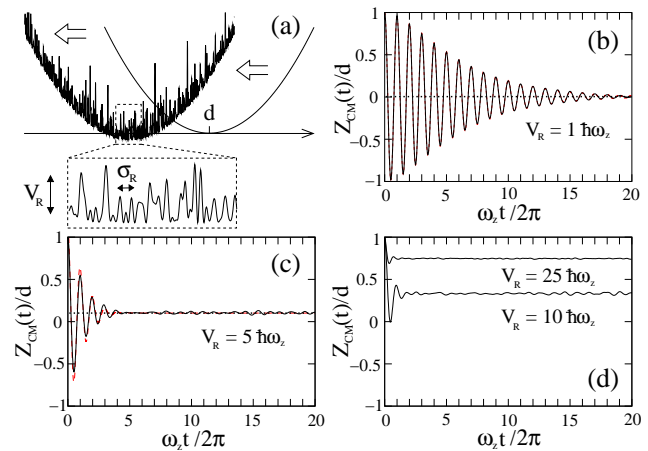


Fig. 1: Dipole oscillations of a 3D elongated ($\lambda = 8$) disordered Fermi gas. a) The oscillations are excited by shifting the trap from $z = d$ to $z = 0$ at time $t = 0$. The disorder is also switched on at $t = 0$. b-d) Dipole oscillations, averaged over 25 realizations of the disorder, for a speckle potential with correlation length $\sigma_R = 0.08 l_z$ and various amplitudes V_R . The solid black lines are exact numerical calculations of $Z_{CM}(t)$ (Eqs. (4),(5)), the dashed red lines are obtained from perturbation theory (Eqs. (1),(7),(8)). Horizontal dotted lines are Eq. (5). Here, we have used $d = 5 l_z$, $T = 0$ and $\mu = 200 \hbar \omega_z$ [20].

^(a)E-mail: lsp@institutoptique.fr

In this work, we study the dipole oscillations of a spin-polarized Fermi gas in a harmonic trap combined with a 1D disordered potential. Dipole oscillations are induced by a sudden displacement of the trap center (see Fig. 1(a)), a technique which is routinely used in experiments with ultracold atoms. We find strong damping even for weak disorder, and identify a metal-insulator crossover when the disorder is increased. We show that for very weak disorder, damping results from dephasing of different modes oscillating with frequencies randomly shifted around the harmonic oscillator frequency. This leads to weakly-damped and almost centered oscillations (see Figs. 1(b) and 1(c)), which are accurately described by perturbation theory. For increasing disorder, the Fermi gas crosses over to a strongly insulating regime, characterized by strongly-damped oscillations with large offset (see Fig. 1(d)). This insulating regime is due to the proliferation of single-particle localized states. So far, dipole oscillations in the presence of disorder have been studied only in BECs [16, 17]. In this case, damping is due to dissipation induced by repulsive interactions [17], a process completely different from the one we identify here for non-interacting Fermi gases.

Framework. – We consider a Fermi gas at thermal equilibrium with temperature T in a 3D axially-symmetric harmonic trap of frequencies ω_z in the longitudinal direction z and ω_\perp in the radial directions x, y (the aspect ratio is $\lambda = \omega_\perp/\omega_z$). The trap is initially centered at $(x, y, z) = (0, 0, d)$. Because of the Pauli exclusion principle, the fermions populate the single-particle eigenstates of the displaced trap, $\Phi_{n_x, n_y, n_z}^{(d)}(x, y, z) = \phi_{n_x, n_y}(x, y)\varphi_{n_z}^{(d)}(z)$, according to the Fermi-Dirac distribution. Here, $|\phi_{n_x, n_y}\rangle$ is the eigenfunction of the radial harmonic trap associated with the eigenenergy $\hbar\omega_\perp(n_x + n_y + 1)$. The function $\varphi_n^{(d)}(z) \equiv \varphi_n(z - d)$ with $\varphi_n(z) = (n!2^n l_z \sqrt{\pi})^{-1/2} \exp(-z^2/2l_z^2) H_n(z/l_z)$ is the eigenfunction of the 1D longitudinal harmonic potential associated with eigenenergy $\epsilon_n = \hbar\omega_z(n + 1/2)$, where $H_n(z)$ is the Hermite polynomial of index n and $l_z = \sqrt{\hbar/m\omega_z}$ the oscillator length in the z -direction. At time $t = 0$, the trap center is abruptly shifted to $z = 0$ and a 1D homogeneous disordered potential, $V(z) = V_R v(z/\sigma_R)$, with average $\langle V \rangle = 0$, amplitude V_R and correlation length σ_R , is switched on (see Fig. 1(a)). In the absence of disorder, this process induces undamped dipole oscillations of the CM along z , $Z_{\text{CM}}(t) = d \cos(\omega_z t)$ [7]. In the presence of disorder, we write the CM motion, averaged over different realizations of the disorder, as

$$Z_{\text{CM}}(t) = Z_{\text{osc}}(t) + Z_\infty, \quad (1)$$

where $Z_{\text{osc}}(t) \sim \Gamma(t) \cos(\omega_z t)$ is the oscillating part with $\Gamma(t)$ an envelope function giving the *damping* of the oscillations and Z_∞ is the oscillation *offset*. In the remainder of the manuscript, we evaluate the quantities $\Gamma(t)$ and Z_∞ and identify their physical origin.

Using the density-matrix formalism, the CM motion reads $Z_{\text{CM}}(t) = \text{Tr}[\hat{z}e^{-i\hat{\mathcal{H}}t/\hbar} \hat{\rho}_{\text{eff}} e^{+i\hat{\mathcal{H}}t/\hbar}]$, where

$$\hat{\mathcal{H}} = -\frac{\hbar^2}{2m} \frac{d^2}{dz^2} + \frac{1}{2} m \omega_z^2 z^2 + V(z) \quad (2)$$

is the single-particle Hamiltonian along the z axis, and $\hat{\rho}_{\text{eff}}$ is an effective density matrix. The expression of $\hat{\rho}_{\text{eff}}$ is obtained by tracing out the radial degrees of freedom, which is possible because the 3D Hamiltonian is spatially separable and unchanged in the x, y directions at $t = 0$. We find

$$\hat{\rho}_{\text{eff}} = \sum_n \frac{f_{\text{eff}}^n(T, \mu, \lambda)}{N} |\varphi_n^{(d)}\rangle \langle \varphi_n^{(d)}|, \quad (3)$$

where the effective Fermi distribution, $f_{\text{eff}}^n(T, \mu, \lambda) = \sum_{n_\perp=0}^{+\infty} \frac{n_\perp + 1}{e^{[\hbar\omega_z(n + \lambda n_\perp) - \mu]/k_B T} + 1}$, includes the occupation numbers of the radial-trap levels [18] and $N = \sum_n f_{\text{eff}}^n(T, \mu, \lambda)$ is the total number of Fermions. In a 3D elongated Fermi gas ($\lambda = \omega_\perp/\omega_z > 1$), the 1D limit is achieved when the population of the transverse excitation modes can be neglected. This occurs for $\hbar\omega_\perp - \mu \gg k_B T$ when $\mu > 0$ and $\mu \gg k_B T$ (degenerate limit) or for $\hbar\omega_\perp \gg k_B T$ when $\mu < 0$ and $|\mu| \gg k_B T$ (classical limit).

To evaluate explicitly $Z_{\text{CM}}(t)$, we use the eigenfunctions $\{|\psi_n\rangle, n \in \mathbb{N}\}$ and the associated eigenenergies $\{E_n\}$ of Hamiltonian $\hat{\mathcal{H}}$. The $Z_{\text{CM}}(t)$ can be decomposed as in Eq. (1) with

$$Z_{\text{osc}}(t) = \sum_{n,p; E_n \neq E_p} e^{-i(E_n - E_p)t/\hbar} \rho_{\text{eff}}^{n,p} \langle \psi_p | \hat{z} | \psi_n \rangle, \quad (4)$$

and

$$Z_\infty = \sum_{n,p; E_n = E_p} \rho_{\text{eff}}^{n,p} \langle \psi_p | \hat{z} | \psi_n \rangle, \quad (5)$$

where the matrix elements $\rho_{\text{eff}}^{n,p} \equiv \langle \psi_n | \hat{\rho}_{\text{eff}} | \psi_p \rangle$ include all the dependency on the parameters of the initial Fermi gas (T, μ, λ) and the trap displacement d . The disordered potential affects the energy spectrum (i.e. both E_n and $|\psi_n\rangle$) of the harmonic oscillator, which, from Eq. (4), appears to have a twofold effect on $Z_{\text{osc}}(t)$. First, it induces random, incommensurate, energy shifts which dephase the different oscillating components of the sum in Eq. (4). As we will see, this is the main contribution to the damping effect for sufficiently weak disorder. Second, it induces random modifications to the harmonic oscillator eigenfunctions, which affect the terms $\langle \psi_p | \hat{z} | \psi_n \rangle$ and $\rho_{\text{eff}}^{n,p}$. According to Eq. (5), these modifications are also responsible for the existence of an oscillation offset, Z_∞ .

Equations (4) and (5) are the basis of both our analytical and numerical calculations. In the numerics, we use a speckle potential similar to that used in many experiments on disordered quantum gases [1, 19], for which the auto-correlation function reads $C(\Delta z) = \langle V(z + \Delta z)V(z) \rangle = V_R^2 c(\Delta z/\sigma_R)$ with $c(u) = (\sin u/u)^2$. Figures 1(b-d) show dipole oscillations of a 3D elongated ($\lambda = 8$) Fermi gas

at zero temperature for various amplitudes V_R [20]. These results show increasing damping for increasing disorder, as expected. More precisely, we find a crossover from *weak-damping* (metal-like) regime for very weak disorder (see Fig. 1(b,c)) to *strong-damping* (insulator-like) regime characterized by a significant offset for stronger disorder (see Fig. 1(d)). As we will show, weak-damping results from disorder-induced weak perturbations of the energy spectrum, while strong-damping signals strong localization of the Fermi gas.

Weak-damping regime. – We first evaluate analytically Z_{osc} from Eq. (4). We take into account first order disorder-induced shifts to the harmonic oscillator eigenenergies and approximate the eigenfunctions $|\psi_n\rangle$ with the harmonic oscillator ones $|\varphi_n^{(0)}\rangle$. Note that, as we will show, the offset Z_∞ requires second-order perturbation calculations. For consistency in Eq. (1), one should in principle use also second-order perturbation for calculating the envelope $Z_{\text{osc}}(t)$. However, it leads to small corrections in $Z_{\text{osc}}(t)$ so we disregard them. We have checked numerically that perturbation of the eigenfunctions has a negligible contribution to the damping, at least until almost complete dephasing has occurred. Then, Eq. (4) is significantly simplified since $\langle\psi_p|\hat{z}|\psi_n\rangle \simeq \langle\varphi_p^{(0)}|\hat{z}|\varphi_n^{(0)}\rangle = \frac{l_z}{\sqrt{2}}(\sqrt{n+1}\delta_{p,n+1} + \sqrt{n}\delta_{p,n-1})$. Using first-order perturbation theory on the eigenenergies E_n only, we find

$$Z_{\text{osc}}(t) = l_z \sum_{n \geq 0} \sqrt{2(n+1)} F_{n,n+1}^{(d)} \cos(\omega_z t + \delta V_n t / \hbar), \quad (6)$$

where $\delta V_n \equiv \langle\varphi_{n+1}^{(0)}|V(z)|\varphi_{n+1}^{(0)}\rangle - \langle\varphi_n^{(0)}|V(z)|\varphi_n^{(0)}\rangle$ and $F_{n,p}^{(d)} \equiv \langle\varphi_n^{(0)}|\hat{\rho}_{\text{eff}}|\varphi_p^{(0)}\rangle$. For different realizations of the disordered potential, δV_n is a random quantity with $\langle\delta V_n\rangle = 0$ and $\langle\delta V_n^2\rangle = V_R^2 \frac{\sigma_R}{l_z} R_n(\sigma_R/l_z)$, where

$$R_n\left(\frac{\sigma_R}{l_z}\right) = \int \frac{d\kappa}{\sqrt{\pi}} \tilde{c}\left(\sqrt{2}\frac{\sigma_R}{l_z}\kappa\right) e^{-\kappa^2} [L_{n+1}^0(\kappa^2) - L_n^0(\kappa^2)]^2$$

is related to the Fourier transform of the reduced correlation function of the disorder, $\tilde{c}(q) = \int \frac{du}{\sqrt{2\pi}} c(u) e^{-iqu}$, and $L_n^\alpha(x)$ are Laguerre polynomials [21]. When averaging Eq. (6) over realizations of the disorder, we use a Gaussian distribution in the variable δV_n with mean square fluctuation $\langle\delta V_n^2\rangle$ [22]. We then find $Z_{\text{osc}}(t) \simeq d\Gamma(t)\cos(\omega_z t)$, where

$$\Gamma(t) = \frac{l_z}{d} \sum_{n \geq 0} \sqrt{2(n+1)} F_{n,n+1}^{(d)} \exp\left[-\frac{V_R^2 t^2}{2\hbar^2} \frac{\sigma_R}{l_z} R_n\left(\frac{\sigma_R}{l_z}\right)\right]. \quad (7)$$

The envelope function $\Gamma(t)$ is non-universal in the sense that its general shape does not depend only on the disorder (i.e. on V_R , σ_R and the model of disorder, v) but also on the initial density matrix, i.e. on temperature (T), number of fermions (or equivalently, chemical potential μ), trap geometry (λ) and initial trap displacement (d). For instance, $\Gamma(t)$ is in general neither an exponential nor a

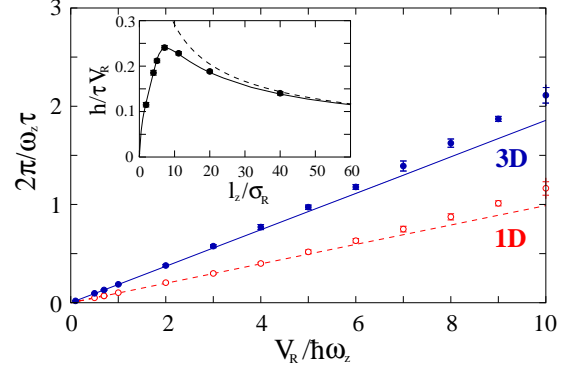


Fig. 2: Damping time, τ , versus V_R in 1D and 3D ($\lambda = 8$) Fermi gases, both for $\mu = 200\hbar\omega_z$ and $\sigma_R = 0.08 l_z$. The inset is τ as a function of σ_R for the 3D gas. The lines are the predictions of Eq. (7) and the points are results of numerical simulations. The dashed line in the inset is the white noise limit. The parameters are $d = 5 l_z$ and $T = 0$.

Gaussian function [23]. To compare Eq. (7) with numerical data, we introduce the *damping time* τ , defined by the equation $\Gamma(\tau) = 1/2$. Although τ depends on both disorder and initial state of the Fermi gas, one can obtain some universal properties from the fact that the contribution of disorder (which appears only in the coefficient of the exponential function in Eq. (7)) is separated from that of the initial state (in the quantities $F_{n,n+1}^{(d)}$ only). In particular, we find $\tau \propto \hbar/|V_R|$ for any model of disorder and initial density matrix. Numerical results for 1D and 3D Fermi gases at zero temperature shown in Fig. 2 confirm this prediction. The behavior of τ versus the correlation length σ_R is more complicated. In the white-noise limit, $\sigma_R \ll l_z/\sqrt{n_F}$, where $n_F = \mu/\hbar\omega_z$ is the longitudinal Fermi level, there are many disorder peaks within the typical wavelength $l_z/\sqrt{n_F}$ of the Fermi gas. The disordered potential felt by the wavefunctions $|\varphi_n^{(0)}\rangle$ with $n \leq n_F$ almost averages out. When σ_R increases, the eigenfunctions are more sensitive to the disorder so that we expect that τ decreases. This behavior is confirmed by Eq. (7): In the white noise limit the functions R_n are independent of σ_R so that $\tau \propto \sqrt{l_z}/\sigma_R$. The coupling of the Fermi gas to the disorder is maximum when $\sigma_R \sim l_z/\sqrt{n_F}$ [24]. Beyond, we thus expect that τ increases. In the limit of large correlation length, $\sigma_R \gg l_z\sqrt{2n_F}$, the typical size of the disorder peaks exceed the size of the Fermi gas. Hence, the disordered potential induces only an energy shift which is approximately equal for all the eigenstates below the Fermi energy, and we recover harmonic oscillations (i.e. $\tau \rightarrow \infty$). This is again confirmed by Eq. (7): Since the width of \tilde{c} is unity we find $R_n(\sigma_R/l_z) \propto (l_z/\sigma_R)^5$ and $\tau \propto (\sigma_R/l_z)^2$. These features explain the non-monotonous behavior of τ versus σ_R obtained in the Inset of Fig. 2.

In contrast to damping, the oscillation offset results only from perturbation on the eigenfunctions $|\psi_n\rangle$ (see Eq. (5)) [25]. Since the average of the disorder vanishes everywhere, $\langle V(z) \rangle = 0$, first-order perturbation is not

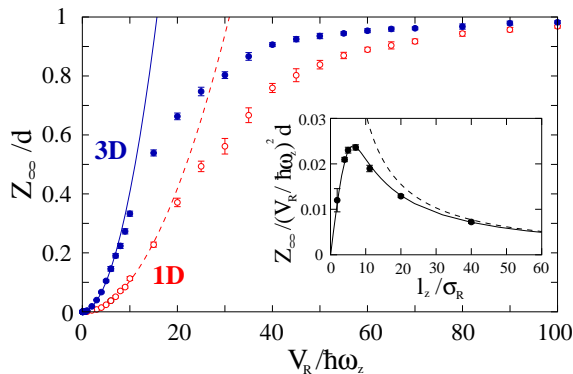


Fig. 3: Oscillation offset, Z_∞ , versus V_R (same parameters as in Fig. 2). The points are results of numerical simulations and the lines are Eq. (8). The inset is Z_∞ as a function of σ_R for the 3D gas. The dashed line is the white noise approximation.

sufficient to calculate the offset. We thus evaluate Eq. (5) up to second order, and find

$$Z_\infty = \left(\frac{V_R}{\hbar\omega_z}\right)^2 \sigma_R \sum_{\substack{n,m \\ n>m}} \sqrt{8\frac{m!}{n!} \frac{F_{n,m}^{(d)}}{n-m}} I_{n,m} \left(\frac{\sigma_R}{l_z}\right), \quad (8)$$

with

$$I_{n,m} \left(\frac{\sigma_R}{l_z}\right) = \int \frac{d\kappa}{\sqrt{\pi}} \tilde{c} \left(\sqrt{2\frac{\sigma_R}{l_z}} \kappa\right) (i\kappa)^{n-m+1} L_m^{n-m}(\kappa^2) \times e^{-\kappa^2} [L_n^1(\kappa^2) - L_m^1(\kappa^2) + L_{m-1}^1(\kappa^2) - L_{n-1}^1(\kappa^2)].$$

As for damping, the behavior of the offset as a function of V_R is simple: we find $Z_\infty \propto (V_R/\hbar\omega_z)^2$ for any initial state of the Fermi gas and trap displacement. This is confirmed, for small enough values of V_R , by the results of numerical calculations plotted in Fig. 3. Again, the dependence of Z_∞ versus σ_R is non-monotonous, as shown in the Inset of Fig. 3. In the white-noise limit, $\sigma_R \ll l_z/\sqrt{n_F}$, we find that $Z_\infty \propto \sigma_R$, while for large correlation length, $\sigma_R \gg l_z\sqrt{2n_F}$, we have $Z_\infty \propto l_z^5/\sigma_R^4$.

Let us comment on two important properties. First, we find that strong damping occurs even for very weak disorder. For instance, $V_R = 5\hbar\omega_z$ (equal to 0.025μ in Figs. 3 and 4) corresponds to $\tau \simeq 2\pi/\omega_z$, meaning that damping occurs typically on few oscillations (see Fig. 1(c)). Second, we find that, for the same chemical potential, the effect of disorder is weaker in 1D than in 3D (the damping time τ is larger and the offset Z_∞ smaller). This can be understood intuitively from the properties of the effective Fermi distribution $f_{\text{eff}}^{n,\mu}(T, \mu, \lambda)$. Indeed, for stronger radial trapping (i.e. for increasing λ or in 1D compared to 3D) and fixed Fermi energy, the population of low-energy states, which are more affected by the disorder, decreases. Similarly, we have found that finite temperature increases the damping time τ and decreases the offset Z_∞ although the effect is quite weak. For instance, we find that a temperature $T = 0.5 T_F$, where T_F is the Fermi temperature, leads to a small correction of about 10%, without affecting the general behavior of τ and Z_∞ versus the parameters.

Note also that the assumptions at the basis of our perturbation approach are justified, *a posteriori*, by the excellent agreement between numerical calculations (points with error bars) and perturbation theory (lines) in Figs. 2 and 3. This is even more striking in Fig. 1(b,c) where we plot the dipole oscillations as obtained independently (i) from exact numerical calculations (based on Eqs. (4),(5); solid black lines) and (ii) from the prediction of Eqs. (1),(7),(8) (dashed red lines). They are hardly distinguished in Fig. 1(b,c), indicating that perturbation theory is indeed very accurate as long as oscillations are visible (i.e. for $V_R \lesssim 5\hbar\omega_z$ for the parameters of Figs. 1-3).

Strong-damping regime and localization. – In the strong-damping regime (i.e. for $V_R \gtrsim 10\hbar\omega_z$ for the parameters of Figs. 1-3), dipole oscillations are largely suppressed (see Fig. 1(d)) and it is difficult to define an envelope function $\Gamma(t)$. At the same time, the offset becomes significant (see Fig. 3) and tends to $Z_\infty \simeq d$ for very large V_R [26]. This behavior signals the crossover to a strongly insulating regime which can be related to the onset of single-particle localization. Indeed, as shown by Eq. (5), the oscillation offset Z_∞ is the sum of the average position of each eigenfunction in the disordered trap, $z_n \equiv \langle \psi_n | \hat{z} | \psi_n \rangle$, weighted by the corresponding population, $\rho_{\text{eff}}^{n,n}$ [25]. Extended states –which are centered around the trap minimum ($z_n \simeq 0$)– do not contribute to Z_∞ . Conversely, localized states which are spread at random positions in the trap, $z_n \neq 0$, may contribute to Z_∞ , depending on their relative population $\rho_{\text{eff}}^{n,n}$.

The two important features that determine the oscillation offset are thus the localization properties of the eigenfunctions in the presence of the harmonic trap, and their populations, which are governed by the initial, displaced Fermi gas. In order to interpret the dipole motion in the strong-damping regime, we now discuss these features. The eigenfunctions $|\psi_n\rangle$ are obtained by numerical diagonalization of Hamiltonian $\hat{\mathcal{H}}$ and characterized by two quantities: (i) the localization center, z_n , and (ii) the participation length, $P_n = 1/\int dz |\psi_n(z)|^4$, which gives the typical extension (width) of the quantum states [27]. Their populations $\rho_{\text{eff}}^{n,n}$ are obtained by projecting the initial state of the Fermi gas on the eigenfunctions $|\psi_n\rangle$. Figure 4 shows all these features for a 1D Fermi gas at $T = 0$, with $\mu = 200\hbar\omega$ and initially centred at $d = 5l_z$. For each eigenenergy E_n , we plot a vertical line of length P_n , centred at position z_n , and weighted by $\rho_{\text{eff}}^{n,n}$ (color scale). The different Figs. 4(a)-(f) correspond to the same realization of a speckle potential but different values of V_R . As can be anticipated, in the weak-damping regime, we find that the eigenfunctions are not localized (see Fig. 4(a)). The values of P_n are close to the participation length P_n^0 calculated for the harmonic trap without disorder (solid blue line). The corresponding z_n slightly fluctuate around the trap center, so that $Z_\infty \ll d$. Increasing the amplitude V_R of the disordered potential (see Figs. 4(b) and 4(c)), most of the populated states remain extended but

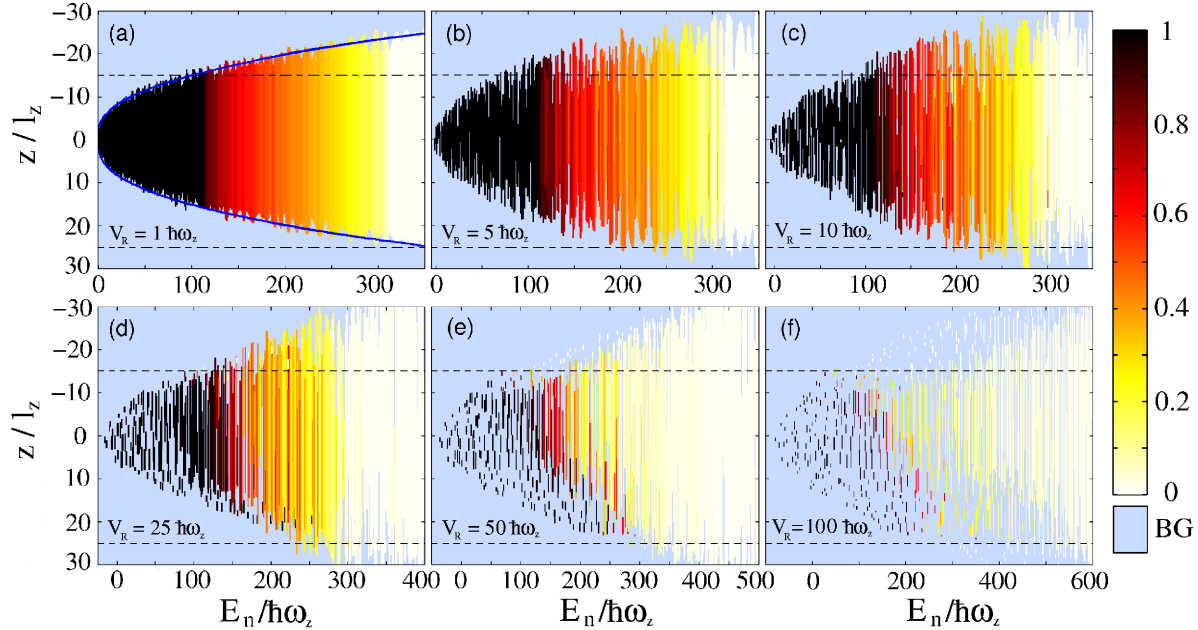


Fig. 4: Localization in a disordered trap. Vertical lines centred in z_n and of length given by the participation length P_n are plotted at energy E_n . The color scale is given by the weight $\rho_{\text{off}}^{n,n}$: it goes from zero (white regions) to one (dark regions). For clarity, the background (BG) is in light blue color. The horizontal dashed lines indicate the spatial region covered by the initial Fermi gas, i.e. $d - l_z\sqrt{2n_F} \leq z \leq d + l_z\sqrt{2n_F}$. The different figures refer to different values of V_R and the same realization of speckle disorder. The solid blue line in Fig. (a) shows the participation length $P_n^{(0)}$ of harmonic oscillator eigenfunctions in the absence of disorder ($V_R = 0$).

become more and more perturbed. In the crossover regime (Figs 4(d) and 4(e)), strongly localized states, randomly distributed in the trap, appear at low energies. The states with lowest energy, which are more sensitive to the disorder and thus more strongly localized, are populated when they lie in the spatial region covered by the initial Fermi gas (delimited by the horizontal dashed lines in Fig. 4). These states, being spatially separated from each other, do not contribute significantly to the sum that determines the oscillation (see Eq. (4)). In contrast, they do contribute to the offset (see Eq. (5)) since they are mostly located on the side of the initial gas. The populated states with higher energy are not localized and extend beyond the spatial region covered by the initial Fermi gas. They can thus contribute to the oscillation, but not significantly to the offset since their average center is close to the trap center. Finally, for very large amplitudes V_R of the disorder (Figs. 4(f)), the Fermi gas enters the strong-damping regime. In this case, most of the populated states are strongly localized and located in the region covered by the initial Fermi gas, with energies about up to the chemical potential. Note that the upper part of Figs. 4(e) and 4(f), above the dashed line, shows states which are strongly localized but not populated since they lie outside the initial Fermi gas. Some extended states with energy above the chemical potential can also appear but with very small population. The CM of the Fermi gas is thus frozen at $Z_{\text{off}} \simeq d$. This explains qualitatively the behavior observed in Fig. 3.

As we have shown, localization is a crucial ingredient for the metal-insulator crossover investigated here. Although localization is mainly due to the disordered potential, it is clear that the harmonic trap significantly affects the localized states. For instance, by virtue of finite-size effects, the lowest-energy states are localized near the trap center (see Figs. 4). Moreover, the exponential decay of localized states, which is the most striking signature of Anderson localization [1, 2], is strongly suppressed since the harmonic potential dominates at large distances. More surprisingly, our numerical data show that localized and extended states can coexist in the same region of the spectrum at intermediate energies (see for instance Figs. 4(d) and 4(e)), an effect due to the trapping potential. In the future, it will thus be interesting to study single-particle localization in disordered traps. On one hand, it differs qualitatively from localization in homogeneous disorder, and, on the other hand, it is directly relevant to experiments on disordered quantum gases.

Conclusions. – Dipole oscillations are an important tool for studying the dynamical properties of ultracold gases [8–17]. We have shown that dipole oscillations of trapped, disordered Fermi gases reveal a metal-insulator crossover for increasing disorder. Weak disorder induces weak-damping associated to weak perturbations of the energy spectrum. Stronger disorder leads to strong-damping characterized by a large oscillation offset, which signals the onset of localization. We have related the insulating prop-

erty of the Fermi gas to localization of energy eigenfunctions in the disordered trap. We have provided analytical predictions in the weak-damping regime and numerical results in the strong-damping regime using experimentally realistic parameters for both 1D and 3D gases. Our predictions can thus be readily tested experimentally with ultracold Fermi gases, in speckle potentials or other models of disorder. Our results can be easily extended to finite temperature Fermi gases, but we have actually found weak differences compared to the zero-temperature case.

This research was supported by the French Centre National de la Recherche Scientifique (CNRS), Agence Nationale de la Recherche (ANR), Ministère de l'Éducation Nationale, de la Recherche et de la Technologie (MENRT), Triangle de la Physique and Institut Francilien de Recherche sur les Atomes Froids (IFRAF).

REFERENCES

- [1] BILLY J., JOSSE V., ZUO Z., BERNARD A., HAMBRECHT B., LUGAN P., CLÉMENT D., SANCHEZ-PALENCIA L., BOUYER P., AND ASPECT A., *Nature (London)*, **453** (2008) 891.
- [2] ROATI G., D'ERRICO C., FALLANI L., FATTORI M., FORT C., ZACCANTI M., MODUGNO G., MODUGNO M., AND INGUSCIO M., *Nature (London)*, **453** (2008) 895.
- [3] SANCHEZ-PALENCIA L., CLÉMENT D., LUGAN P., BOUYER P., SHLYAPNIKOV G.V., AND ASPECT A., *Phys. Rev. Lett.*, **98** (2007) 210401; SANCHEZ-PALENCIA L., CLÉMENT D., LUGAN P., BOUYER P., AND ASPECT A., *New J. Phys.*, **10** (2008) 045019.
- [4] DAMSKI B., ZAKRZEWSKI J., SANTOS L., ZOLLER P., AND LEWENSTEIN M., *Phys. Rev. Lett.*, **91** (2003) 080403; ROTH R. AND BURNETT K., *J. Opt. B: Quantum Semiclass. Opt.*, **5** (2003) S50.
- [5] DUBI Y., MEIR Y., AND AVISHAI Y., *Nature (London)*, **449** (2007) 876.
- [6] BELOBORODOV I.S., LOPATIN A.V., VINOKUR V.M., AND EFETOV K.B., *Rev. Mod. Phys.*, **79** (2007) 469.
- [7] KOHN W., *Phys. Rev.*, **123** (1961) 1242; DOBSON J.F., *Phys. Rev. Lett.*, **73** (1994) 2244.
- [8] DALFOVO F., GIORGINI S., PITAEVSKII L.P., AND STRINGARI S., *Rev. Mod. Phys.*, **71** (1999) 463.
- [9] GIORGINI S., PITAEVSKII L.P., AND STRINGARI S., *Rev. Mod. Phys.*, **92** (2008) 1215.
- [10] MORITZ H., STÖFERLE T., KÖHL M., AND ESSLINGER T., *Phys. Rev. Lett.*, **91** (2003) 250402.
- [11] FERTIG C.D., O'HARA K.M., HUCKANS J.H., ROLSTON S.L., PHILLIPS W.D., AND PORTO J.V., *Phys. Rev. Lett.*, **94** (2005) 120403.
- [12] PEZZÉ L., PITAEVSKII L., SMERZI A., STRINGARI S., MODUGNO G., DE MIRANDES E., FERLAINO F., OTT H., ROATI G., AND INGUSCIO M., *Phys. Rev. Lett.*, **93** (2004) 120401.
- [13] HOOLEY C. AND QUINTANILLA J., *Phys. Rev. Lett.*, **93** (2004) 080404; RUUSKA V. AND TÖRMÄ P., *New J. Phys.*, **6** (2004) 59; KENNEDY T.A.B., *Phys. Rev. A*, **70** (2004) 023603; RIGOL M. AND MURAMATSU A., *Phys. Rev. A*, **70** (2004) 043627.
- [14] SCAROLA V.W. AND DAS SARMA S., *Phys. Rev. A*, **73** (2006) 041609(R).
- [15] STROHMAIER N., TAKASU Y., GÜNTER K., JÖRDENS R., KÖHL M., MORITZ H., AND ESSLINGER T., *Phys. Rev. Lett.*, **99** (2007) 220601; OTT H., DE MIRANDES E., FERLAINO F., ROATI G., MODUGNO G., AND INGUSCIO M., *Phys. Rev. Lett.*, **92** (2004) 160601.
- [16] LYE J.E., FALLANI L., MODUGNO M., WIERSMA D., FORT C., AND INGUSCIO M., *Phys. Rev. Lett.*, **95** (2005) 070401; MODUGNO M., *Phys. Rev. A*, **73** (2006) 013606; FALCO G.M., PELSTER A., AND GRAHAM R., *Phys. Rev. A*, **76** (2007) 013624; CHEN Y.P., HITCHCOCK J., DRIES D., JUNKER M., WELFORD C., AND HULET R.G., *Phys. Rev. A*, **77** (2008) 033632.
- [17] ALBERT M., PAUL T., PAVLOFF N., AND LEBOEUF P., *Phys. Rev. Lett.*, **100** (250405) 2008.
- [18] Here, the zero-point energy, $\hbar\omega_z(1/2 + \lambda)$, has been included into the definition of the chemical potential μ .
- [19] CLÉMENT D., VARON A.F., RETTER J.A., SANCHEZ-PALENCIA L., ASPECT A., AND BOUYER P., *New J. Phys.*, **8** (2006) 165.
- [20] The numerics have been carried out for typical parameters of ^{40}K experiments [12]: $\lambda = 8$, $l_z = 3.25 \mu\text{m}$ so that $\mu = 200 \hbar\omega_z$ corresponds to $N \approx 20000$ atoms. For the speckle potential, we have used $\sigma_R = 0.26 \mu\text{m}$ as in the experiments of Ref. [1].
- [21] ABRAMOWITZ M. AND STEGUN I.A., *Handbook of Mathematical Functions* (Dover, New-York) 1964.
- [22] We have checked numerically that this approximation is very accurate. However complete justification of this property is beyond the scope of the present paper.
- [23] A Gaussian envelope can be obtained in the particular case of a 1D Fermi gas at $T = 0$ in the small d limit. To first order perturbation in the displacement d , we have $|\varphi_n^{(d)}\rangle \simeq |\varphi_n^{(0)}\rangle + \frac{d}{\sqrt{2}l_z}(\sqrt{n+1}|\varphi_{n+1}^{(0)}\rangle - \sqrt{n}|\varphi_{n-1}^{(0)}\rangle)$ and $F_{n,n+1} = \frac{d}{\sqrt{2}l_z} \frac{\sqrt{n+1}}{N} (f_{\text{eff}}^n(T, \mu, \lambda) - f_{\text{eff}}^{n+1}(T, \mu, \lambda))$. In 1D and at $T = 0$, we have $N = n_F + 1$ and $F_{n,n+1} = \frac{d}{l_z} \frac{1}{\sqrt{2(n_F+1)}} \delta_{n,n_F}$, where n_F is the Fermi level. In this case only, oscillations are undamped for each realization of the disorder with a frequency shift δV_{n_F} . Then, damping results from averaging over disorder and $\Gamma(t) = \exp\left[-\frac{V_R^2 t^2}{2\hbar^2} \frac{\sigma_R}{l_z} R_{n_F}\left(\frac{\sigma_R}{l_z}\right)\right]$ is a simple Gaussian. Note however that this limiting case is valid only for very small displacement, i.e. $d \ll l_z/\sqrt{n_F}$.
- [24] Analogous non-monotonic behavior can be found when evaluating the parameter δV_n as a function of σ_R .
- [25] Equation (5) shows that the offset is mainly determined by components with $n = p$. In fact, there may be additional contributions due to degeneracies in the spectrum (i.e. contributions with $n \neq p$ but $E_n = E_p$). This case is very unlikely in fully disordered potentials so we neglect such contributions. Degeneracy-induced offset is instead relevant for symmetric optical lattices [12, 13].
- [26] For the numerical calculation of this section we consider the condition of optimal coupling between the Fermi gas and the disordered potential, $\sigma_R \sim l_z/\sqrt{n_F}$.
- [27] For normalized states, i.e. $\int dz |\psi_n(z)|^2 = 1$, small participation lengths correspond to strongly localized states.